European Polymer Journal 153 (2021) 110493

Contents lists available at ScienceDirect

European Polymer Journal

journal homepage: www.elsevier.com/locate/europolj

Accelerated photodegradation of polystyrene by TiO_2-polyaniline photocatalyst under UV radiation

S. Dinoop lal [a], T. Sunil Jose [a,*], C. Rajesh [b], P. Anju Rose Puthukkara [a], K. Savitha Unnikrishnan [a], K.J. Arun [c]

[a] Dept. of Chemistry, St.Thomas' College, Thrissur, Kerala 680 001, India
[b] Dept. of Chemistry, MES Keveeyam College, Valanchery, Malappuram, Kerala PIN: 676552, India
[c] Department of Physics, Sree Kerala Varma College, Thrissur, Kerala PIN: 680011, India

ARTICLE INFO

Keywords:
Nano TiO_2-PANI composites
Polystyrene
Photodegradation
Break down voltage
Dielectric permittivity
Mechanical properties

ABSTRACT

Photodegradation of polystyrene (PS) was studied under ultraviolet (UV) radiation, using nano TiO_2, surface modified with polyaniline (PANI). X-Ray diffractogram reveals that the crystalline structure of TiO_2 remained intact in TiO_2-PANI composites. The existence of strong molecular interaction between TiO_2 and PANI lead to a decrease in the optical bang gap energy of TiO_2 in the composites. PS loaded with TiO_2-PANI composites underwent better chain scission and photo-oxidation compared to PS and PS-TiO_2 composites, upon UV irradiation. TiO_2-PANI composites enhanced the mechanical properties (tensile and flexural) of PS appreciably. Tensile and flexural strengths however decreased with respect to UV exposure time, proving mechanical deterioration of the polymer composites as an outcome of photodegradation. Thermal stability of the composites too decreased upon UV exposure. A decrease in the values of break down voltage as well as increase in dielectric permittivity of the composites upon UV irradiation suggests the formation of charge centers and polarisable species in the polymer matrix. All the polymer composites underwent considerable weight loss due to the formation and evolution of volatile gases, during the course of photodegradation. Suitable mechanism of degradation of PS composites was proposed based on the observed results.

1. Introduction

20th century witnessed rapid growth in plastic production worldwide [1]. The global production of plastics was estimated to be around 2 metric tons in 1950 [2]. The total quantity of plastic produced between the years 1950 and 2018 was around 6 billion tons. Out of these only 21% has been incinerated or recycled, while the remaining 79% were left untreated [3]. Disposable plastic commodities comprises 50% of the total plastics ever produced [4]. Increase in the global plastic production, lead to an increase in the concentration of plastic debris spread across the world, threatening the ecosystem seriously [5]. Even though most of the commodity plastics like polystyrene, polypropylene, polyethylene, polyvinyl alcohol, polymethyl methacrylate etc are non-biodegradable, they could be degraded photochemically. The so called photodegradation, even though a slow process, could be considered a safe method for the demolition of polymer debris. The process neither requires additional expensive energy nor does produce any hazardous side products during the course. Photodegradation causes chain dissociation in polymers along with oxidation. The physical, chemical, mechanical, electrical and optical properties of the polymer are severely affected after photodegradation [6,7]. Macromolecular residue left behind after the process could undergo biodegradation much easily. Photodegradation could be implemented as a common system of plastic waste treatment only if the entire process proceeds in a stipulated time. Introducing photocatalysts/ photosensitizers could efficiently accelerate the rate of photodegradation. This work mainly studies the accelerated photodegradation of polystyrene (PS) under ultraviolet (UV) radiation in the presence of surface modified nano TiO_2 as photocatalyst. Surface modification of TiO_2 has been done by coupling it with polyaniline (PANI).

TiO_2 is an extensively studied versatile photocatalyst used in various applications including environmental remedial measures [8,9]. Satisfactory results were obtained when TiO_2 was used as photocatalyst for polymer degradation [10–12]. TiO_2 absorbs UV radiation of solar spectra, owing to its optical band gap energy ranging between 3.2 and 3.5 eV, resulting in electron-hole pair separation between valence band

* Corresponding author at: Department of Chemistry, St. Thomas' College (Affiliated to University of Calicut), Thrissur, Kerala PIN: 680 001, India.
E-mail address: suniljosestc@gmail.com (T. Sunil Jose).

https://doi.org/10.1016/j.eurpolymj.2021.110493
Received 19 March 2021; Received in revised form 18 April 2021; Accepted 26 April 2021
Available online 11 May 2021

(VB) and conduction band (CB). Photochemistry of TiO_2 entirely depends upon the transport of these separated electrons that are excited from VB to CB to another molecule or species in its vicinity [13]. Successful interaction of these free electrons with another species before recombination with holes that are left behind in VB may result in photocatalytic reaction. The photocatalytic efficiency of TiO_2, however cannot be fully utilized due to charge recombination. Modification of TiO_2 using some other materials/ molecules/ sensitisers can check the fast recombination of charges.

One of the effective methods that could be employed for the enhancement of photocatalytic activity of semiconductor metal oxides like TiO_2 is, coupling them with a suitable conjugated system [14,15]. Inorganic semiconductors blended with conducting polymers have gained much attention due to their widespread applications which include photocatalysis [16,17]. Conjugated polymers like polyaniline (PANI) have been of quite interest to the researchers due to its astonishing chemistry and physics [18]. The advantages of PANI include high stability in environment due to conjugation, high efficiency in carrying charges, low cost, ease for preparation etc. Due to these reasons PANI has been adopted in various fields of applications including photochemistry [19], electrochemistry [20], optics [21], biosensing [22] etc. The photochemistry of semiconductor metal oxides which are limited to UV region could be extended to visible region also, upon blending them with PANI. The extended π-conjugation of PANI which can exchange charge carriers with semiconductor metal oxides to which they are blended is the primary reason for this. TiO_2 behaves like n-type semiconductor [23] and PANI is considered as p-type semiconducting polymer [24]. The combination of p-type PANI semiconductor with n-type TiO_2 semiconductor hence opens up the path for developing new hybrid composites with good capacitance property and stability [25]. TiO_2-PANI blend exhibit enhanced photocatalytic behavior [26–29]. PANI acts as photosensitizer that can enhance the photocatalytic efficiency of TiO_2 to which it is associated. As PANI can absorb in UV as well as visible region of the spectra, incorporation of PANI into TiO_2 can reduce the band gap energy [30]. Surface modified TiO_2 using PANI could hence bring about better quantum yield.

2. Materials and methods

Nano TiO_2 (25 nm) was purchased from Sigma Aldrich, polystyrene beads were purchased from LG Polymers India Pvt. Ltd. and aniline was purchased from Merck India Pvt. Ltd. The melt flow index of polystyrene is 9 g/10 min (test condition: 200 °C/5Kg; Test method (ASTM): D 1238 'G'). Toluene, hydrochloric acid and deionised water were used as solvents. Ultraviolet (UV) lamp of power 30 W and wavelength 253 nm (Philips Holland) was used as UV source.

2.1. Preparation of PANI and TiO_2-PANI composites

Polyaniline (PANI) was synthesized by chemical oxidative polymerization method. Typically 1.25 ml of aniline was dissolved in 125 ml HCl (1 M) solution in a beaker (beaker A) and stirred for 15 min using a magnetic stirrer. 3.125 g of ammonium peroxodisulphate (APS) was simultaneously dissolved in 125 ml HCl (1 M), in another beaker (beaker B) and stirred for 15 min. Contents in beaker 'B' was added drop wise into beaker 'A' with vigorous stirring over an ice bath. The beaker was then kept under stirring for 12 h. The green coloured solid mass was filtered out from solution. This was then washed using acetone followed by distilled water several times. The dark green solid mass hence obtained was dried at 60 °C for 12 h and ground into fine powder [31–34].

TiO_2-PANI nanocomposites were developed by insitu polymerisation of aniline over dispersed TiO_2 via chemical oxidative polymerization. Number of moles of nano TiO_2 and aniline taken were varied in order to get composites with varying mole percentages. In order to prepare TiO_2-3% PANI composite (3 mol percentage of PANI with respect to TiO_2), 0.034 ml of aniline was dissolved in 35 ml (1 M) HCl in beaker 'A' and stirred for 15 min. 0.966 g of nano TiO_2 was added into the beaker slowly and by vigorous stirring. The mixture was sonicated using probe sonicator for 30 min. Simultaneously, 0.086 g of APS was dissolved in 35 ml (1 M) HCl and stirred for 15 min in another beaker (B). Beaker 'A' was immediately transferred into an ice bath with vigorous stirring and the contents of beaker 'B' was added drop wise into beaker 'A'. The mixture was stirred vigorously for 12 h. Green solid mass was filtered out from the solution, washed with acetone followed by distilled water and dried for 12 h at 60° C [35]. TiO_2-10% PANI and TiO_2-30% PANI were prepared similarly, varying the mole percentages of TiO_2 and PANI in each case as give in table 1.

Table 1
Mole percentages and weights of the components in TiO_2-PANI composites.

Composite	TiO_2 Mole %	PANI Mole %	Weight of nano TiO_2 (g)	Volume of aniline (ml)	Weight of APS in (g)
TiO_2 + 3% PANI	97	3	0.966	0.034	0.086
TiO_2 + 10% PANI	90	10	0.886	0.114	0.286
TiO_2 + 30% PANI	70	30	0.657	0.343	0.857

2.2. Preparation of PS-composite sheets

PS composite sheets were prepared by solvent casting method [36]. 3 wt% of photocatalyst was added to PS dissolved in toluene. The viscous solution was homogenised using a 750 Watt ultrasonic probe sonicator for 40 min, poured into petri dishes and kept in a vacuum oven for 12 h. The specimens were allowed to dry under ambient condition for 7 days. PS-composite sheets hence obtained were exposed to UV radiation for photodegradation. PS loaded with 3 wt% nano TiO_2 was found to exhibit maximum mechanical strength (Fig. S1) and for the same reason, photocatalyst loading was optimized to be 3% throughout the study.

2.3. Preparation of PS-composite specimens for mechanical and electrical measurements

Finely chopped PS and PS composite sheets, prepared by solvent casting method were fed into an injection moulder (Windsor, India), in order to obtain specimens for tensile strength as per *ISO-527–2-1A* standard and flexural strength as per *ISO-178* standard (Supporting data Fig. S2). Specimens for break down voltage (BDV) determination were moulded using a hydraulic hot press. Disc shaped specimens of uniform thickness (1 mm) and diameter (75 mm) were obtained. All the samples for mechanical strength and BDV determination subjected to UV irradiation. Tensile and flexural strengths of UV irradiated samples were measured using a universal testing machine (UTM). BDV of respective specimens, after UV irradiation were measured using a specially designed measurement setup as explained in section 2.5. Tensile, flexural and BDV measurements were conducted for a set of three samples each.

2.4. Setup for photodegradation of PS-composites

PS composites were exposed to UV radiation in a wooden chamber with ample air supply. The chamber consisted of a UV tube of wavelength 253 nm and power 30 W. The PS composite specimens and the UV tube were separated by a distance of 8 cm. All the specimens were irradiated for 1000 h and at each regular interval of 200 h the specimens were monitored using various techniques as discussed below.

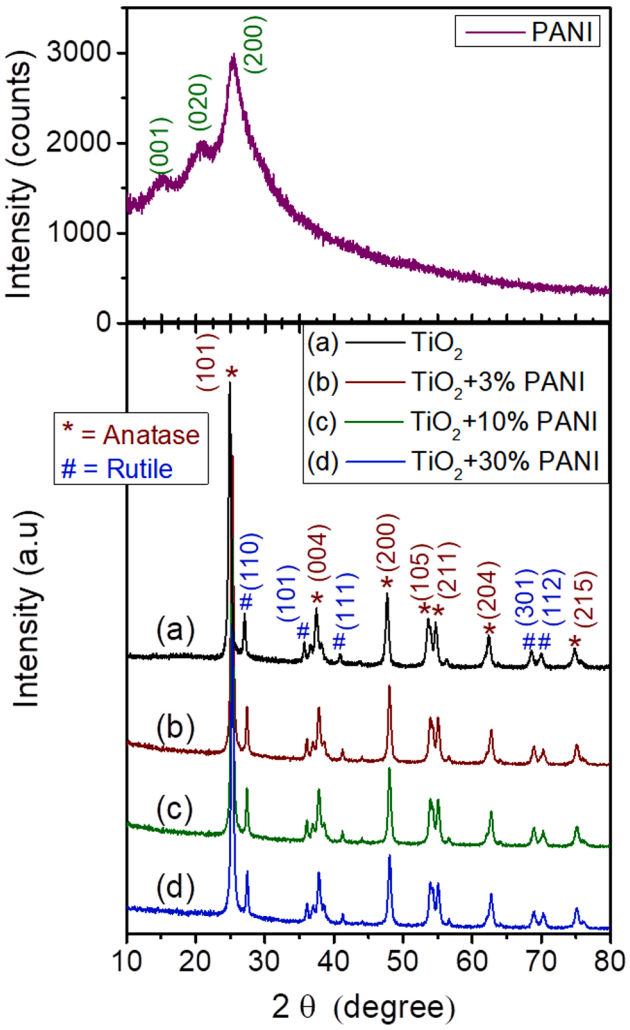

Fig. 1. XRD pattern of PANI, TiO_2 and TiO_2-PANI composites.

2.5. Instrumentation

X-ray diffractogram of the photocatalysts were obtained using X-ray diffractometer (XRD), Aeris, Panalytical. The source of X-ray was Copper-K alpha radiation having wavelength 1.5406Å. High resolution transmission electron microscope (HRTEM), JEM 2100, Jeol was used to study the particle size and morphology of the photocatalysts. Selected area electron diffraction (SAED) patterns were also obtained using the same instrument. Energy dispersive X-Ray (EDX) instrument, JED 2300, Jeol, was used to analyse the elements present in the prepared photocatalysts. Structural analysis was done using FTIR spectrometer, IRAffinity-1S, Shimadzu, Japan. The photocatalysts as well as polymer sheets were directly subjected to FTIR analysis without any sample preparation, using the FTIR spectrometer, working in attenuated total reflection (ATR) mode. UV–visible spectra of the specimens were measured directly using UV–visible diffused reflectance spectrophotometer (UV-DRS), UV-2600, Shimadzu, Japan. $BaSO_4$ powder was used as reference sample. Gel Permeation Chromatography (GPC) was used to determine the average molecular weight of the polymer specimens. The GPC instrument used was LC-20AD, Shimadzu, Japan with silica gel as the stationary phase and tetrahydrofuran as mobile phase. Mechanical properties of the polymer composites were measured using a universal testing machine (UTM), Autograph AG-X plus, Shimadzu, Japan. All the polymer specimens were moulded and conditioned according to ISO standards, before measuring their mechanical properties. Thermogravimetric analysis (TGA) of the specimens was done using the instrument, STA 6000, Perkin Elmer, under nitrogen atmosphere. Surface image of the polymer specimens were obtained using scanning electron microscope (SEM), JSM-6390LV, JEOL. Impedance Analyser, Keysight Technologies E4990A, was used to measure the capacitance of the polymer specimens, between the frequency range 20 and 10^7 Hz. Dielectric constant of the specimens was calculated from these measured capacitance values. Dielectric breakdown or break down voltage (BDV) was measured using specially designed wooden chamber with two copper electrodes aligned in a head to head fashion with respect to each other (Supporting data Fig. S3). The electrodes were connected to the two terminals of a high power alternating current (AC) voltage source. The disc shaped sample (1 mm thickness) was placed in between the round heads of the electrodes. The chamber was filled with transformer oil so as to immerse the electrodes and sample completely. Transformer oil served as insulator in order to suppress arcing or discharges of electricity which may lead to current leakage and false measurement. Voltage needed to break the sample (BDV) was measured for the polymer samples and their duplicates.

3. Results and discussion

3.1. Characterization of photocatalysts

X-ray diffraction peaks of the synthesized PANI observed at 2θ angles 15.16°, 21.11° and 25.59° correspond to characteristic crystal planes (011), (020) and (200) of PANI respectively (Fig. 1.) [37]. The peak at $2\theta = 21.11°$ could be ascribed to PANI chains arranged parallel to each other (characteristic distance between two chains holding benzene ring parallel to each other) while $2\theta = 25.59°$ represents perpendicular arrangement of the polymer chain [38]. The relative higher intensity of $2\theta = 25.59°$ peak in comparison with that of $2\theta = 21.11°$ proves the existence of PANI as emeraldine salt [39]. In addition to these three peaks, another less intense broad peak observed at $2\theta = 9.03°$ represents highly ordered structure (crystalline nature) of PANI where d spacing is high [40].

Diffractogram of TiO_2 showed its existence predominantly in anatase phase with fewer rutile phase [10,36]. XRD patterns of TiO_2-PANI composites resembled that of pristine TiO_2. The presence of PANI could not be identified in the diffractogram of TiO_2-PANI composites. Hampering of crystal growth of PANI by TiO_2 may be the reason for the observation [29]. TiO_2 particles hamper free chain growth of PANI by adsorbing them over TiO_2 surface and tethering their chains leading to a decrease in the degree of crystallinity of PANI, during the process of composite formation [41,42]. Crystallite sizes, determined using Scherrer's formula [43] for TiO_2, TiO_2 + 3%PANI, TiO_2 + 10%PANI and TiO_2 + 30%PANI were 18.9, 20.5, 20.7 and 20.8 nm respectively. Increased percentage of PANI loading thus increased the crystallite size of the composites. Inter planar distance (d) calculated using Bragg's equation for TiO_2-PANI composites (Supporting information Table S1) showed not much appreciable change compared to that of pristine TiO_2. It could be assumed that the crystal morphology of TiO_2 is not much affected by PANI incorporation.

EDX spectra (Fig. 2 A) showed that the composite was pure without any other impurities. EDX peaks observed at 4.5, 4.93 and 0.45 keV represent the Kα1, Kβ1 and Lα1 peaks of titanium respectively. EDX peaks corresponding to oxygen and carbon were also observed at 0.53 (Kα1) and 0.277 (Kα1) keV respectively. EDX peak for nitrogen which was supposed to appear at 0.392 (Kα1) was not visible due to the overlap of carbon and titanium peaks with the less intense peak of nitrogen. HRTEM image of TiO_2 + 10% PANI composite revealed its crystalline morphology, without much aggregation (Fig. 2 B). Particle size ranged between 20 nm and 60 nm. At higher resolution, lattice fringes with 0.35 nm spacing were visible (Fig. 2 C). These patterns represent the inter planar distance (d) corresponding to (101) crystal planes of nano TiO_2. Selected area electron diffraction (SAED) pattern of the composite (Fig. 2 D) further confirms its crystalline nature through the

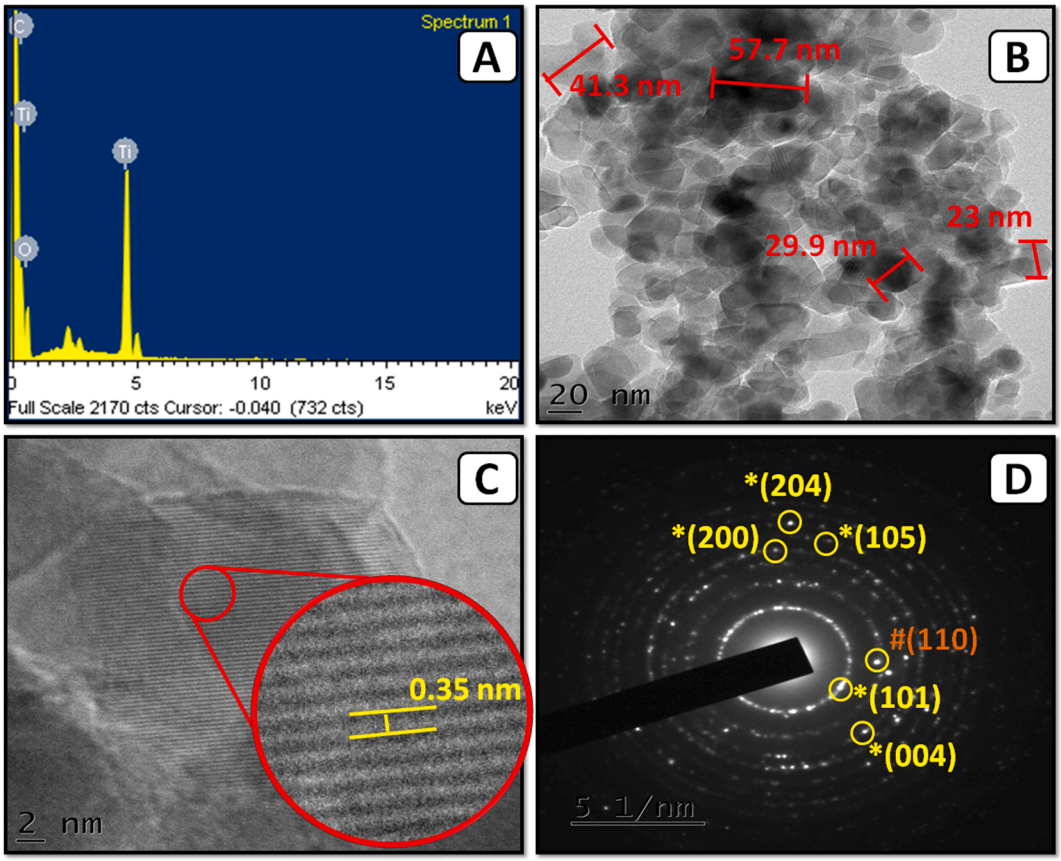

Fig. 2. EDX (A), HRTEM image (B&C) and SAED pattern (D) of nano TiO_2-10% PANI composite.

distinguishable spots over clear ring patterns. Crystal planes corresponding to some of these spots were identified by comparing them with XRD patterns as marked in the figure.

FTIR spectra of PANI showed peaks at 1527 and 1409 cm^{-1} corresponding to N = Q = N and N-B-N stretching frequencies respectively ['Q' represents quinoid and 'B' represents benzenoid structures] (Fig. 3). The coexistence of quinoid and benzenoid structures in PANI was hence evident. Peaks at 1265, 1226 and 1069 cm^{-1} corresponds to secondary aromatic amine C-N stretching, C-$N^{+\bullet}$ polaron stretching and N-H stretching vibrations in charged polaron units respectively. Broad peak between 881 and 690 cm^{-1} originated from C-H in plane bending of 1,4-disubstituted benzene ring. The peak observed at 1710 cm^{-1} corresponds to C = N stretching vibration of imine group due to the presence of quinoid units in PANI. Peaks around 3617 and 3000 cm^{-1} arose from N-H and C-H stretching vibrations respectively. The predominance of quinoid structure over benzenoid structure in PANI was clear from the observed high intense peak of N = Q = N stretching frequency compared to that of N-B-N. This observation further revealed the presence of HCl doped PANI [37,44,45]. IR spectra of TiO_2-PANI composite exhibited all the vibration peaks corresponding to pristine PANI and TiO_2. The intensity of absorption peak belonging to N = Q = N was weaker compared to N-B-N in TiO_2-PANI composites. As the percentage of PANI decreased in TiO_2-PANI composites, intensity of N = Q = N stretching vibrations decreased. The intensities of C-N, C-$N^{+\bullet}$ polaron as well as C = N stretching vibrations were weak in TiO_2-PANI composites. The characteristic absorption bands of PANI, also underwent a considerable shift in peak positions upon coupling with TiO_2. All these observations indicate molecular interaction between TiO_2 and PANI.

UV–visible diffused reflection spectra (UV-DRS) of PANI gave three major characteristic absorption bands (Fig. 4 A). The band observed in the UV region with maximum absorption at 276 nm could be attributed to the transition of electron from π (HOMO) to π* (LUMO) orbitals of benzenoid rings (also called exciton transition). A broad band with absorption maxima 418 nm arose due to polaron to π* electron transition. This absorption band confirms the presence of polarons (C-$N^{+\bullet}$) in the PANI chain as a result of HCl doping. Another broad band with absorption maximum observed at 632 nm attributed to the π to polaron transfer within PANI. This band also represents localized electrons in PANI [46].

UV-DRS of TiO_2-PANI composites exhibited the bands corresponding to TiO_2 as well as PANI with slight peak shifts. The peak observed at 276 nm for pristine PANI was completely masked by the bands of TiO_2 in the same region. The peak around 418 nm observed in PANI was slightly red shifted. This reveals the fact that the polaron to π* transfer in PANI was interrupted through the association of PANI with TiO_2. Another striking observation was that the absorption band around 632 nm in PANI was completely reconstructed in TiO_2-PANI composite with an endless long tail peak starting from around 480 nm. The "free-carrier-tail"[38] attributes to the extended delocalization of electrons, arising due to the expansion of PANI chain in association with TiO_2. In other words, the compact conformation of PANI chain due to strong interactions within the chain which gave a band at around 632 nm for PANI, was modified in the presence of TiO_2 into an expanded conformation. This expanded conformation resulted in better delocalization of charge carriers and interaction with isolated polarons leading to a "tail band" extending beyond the far-red region of the spectra in TiO_2-PANI composites. It should also be noted from the UV–visible spectra that the band intensities corresponding to polaron was decreased in TiO_2-PANI composites. Even though the presence of TiO_2 extended the chain conformation of PANI, the intensities of peaks arising due to polaron structure decreased as the percentage of TiO_2 in the composites increased from TiO_2-30% PANI to TiO_2-3% PANI. This observation supports the conclusion revealed from FTIR spectra that the polarons decreased in the composites as percentage of TiO_2 increased.

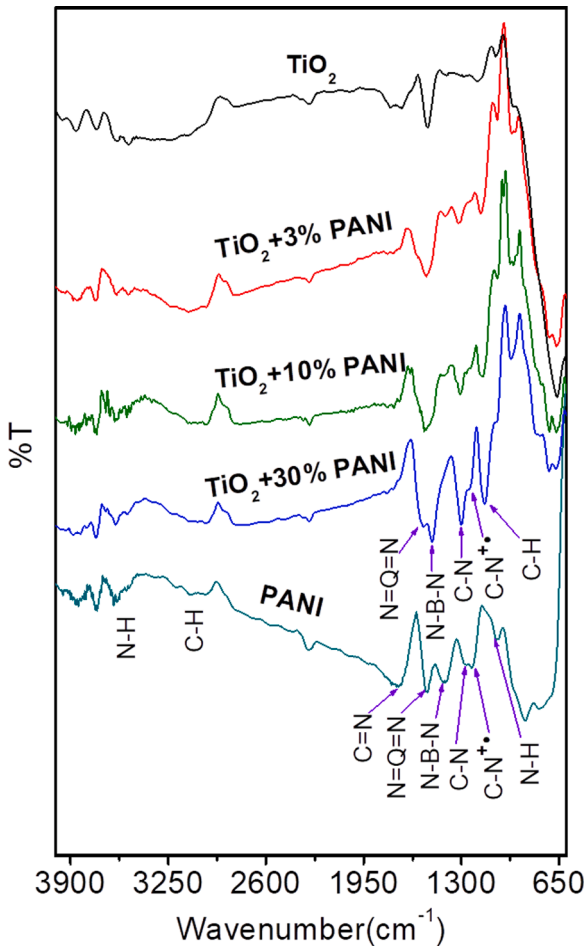

Fig. 3. FTIR spectra of TiO_2, PANI and TiO_2-PANI composites,

Optical band gap energy of TiO_2 and TiO_2-PANI composites were determined from Tauc plote, where, Kubleka-Munk function (F(R)) replaces extinction coefficient (α) to obtain *modified Kubleka-Munk function* as represented in equ 1.

$$F(R)h\upsilon = A(h\upsilon - E_g)^n \quad (1)$$

Where, $F(R)$ = Kubleka-Munk function, R = reflectance, E_g = optical band gap energy, h = Planks constant and ν = frequency of radiation ($h\nu$ represents the energy of photon). The constant n represents the type of transition (direct or indirect).

F(R) was determined from the reflectance spectra of TiO_2 and TiO_2-PANI composites using the relation given below (equ 2)

$$F(R) = (1-R)^2/2R \quad (2)$$

The plot of $(F(R).h\nu)^2$ versus $h\nu$, gives the direct allowed optical band gap energy (E_g) as shown in Fig. 4 B. It was found that E_g of TiO_2-PANI composites were lower than pristine TiO_2. The value of E_g decreased in the composites as the percentage of PANI increased. The observed trend in the values of E_g (Table 2) implies that, band gap energy of TiO_2 decreased upon coupling with PANI.

3.2. Monitering photodegradation

Observations and conclusions made from various monitoring techniques used for the study of photodegradation of PS and PS-composites under UV radiation are as discussed below.

The average molecular weights (weight average $\overline{M}_w$ and number average$\overline{M}_n$ molecular weights) measured for PS, PS-TiO_2 and PS-TiO_2-PANI composites using GPC, seemed to have decreased as the time of UV irradiation is increased (Fig. 5 A). It is clear from Fig. 5 A that PS-TiO_2-PANI composites showed better decrease in average molecular weight compared to PS-TiO_2 as well as PS. Better decrease in the values of $\overline{M}_w$ and$\overline{M}_n$ was observed in PS-3% (TiO_2-10% PANI) composites compared to PS-3% (TiO_2-3% PANI) and PS-3% (TiO_2-30% PANI) composites. The determination of number of chain scissions per molecules (S), number of scission events per gram (N_t) and polydispersity index (PDI) were made from $\overline{M}_w$ and$\overline{M}_n$ following the equations (3), (4) and (5) respectively [36].

Table 2
Values of optical band gap energy of TiO_2 and TiO_2-PANI composites in eV.

	E_g (eV)
TiO_2	3.21
TiO_2 + 3%PANI	*2.90*
TiO_2 + 10%PANI	*2.48*
TiO_2 + 30%PANI	*2.26*

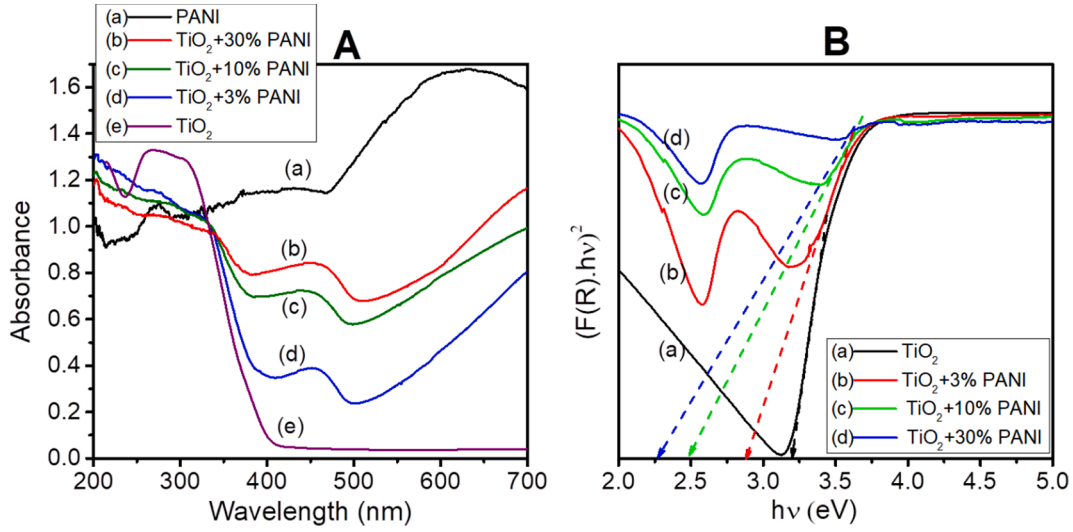

Fig. 4. A) UV-DRS and B) $(F(R).h\nu)^2$ v/s $h\nu$ plote of TiO_2, PANI and TiO_2-PANI composites.

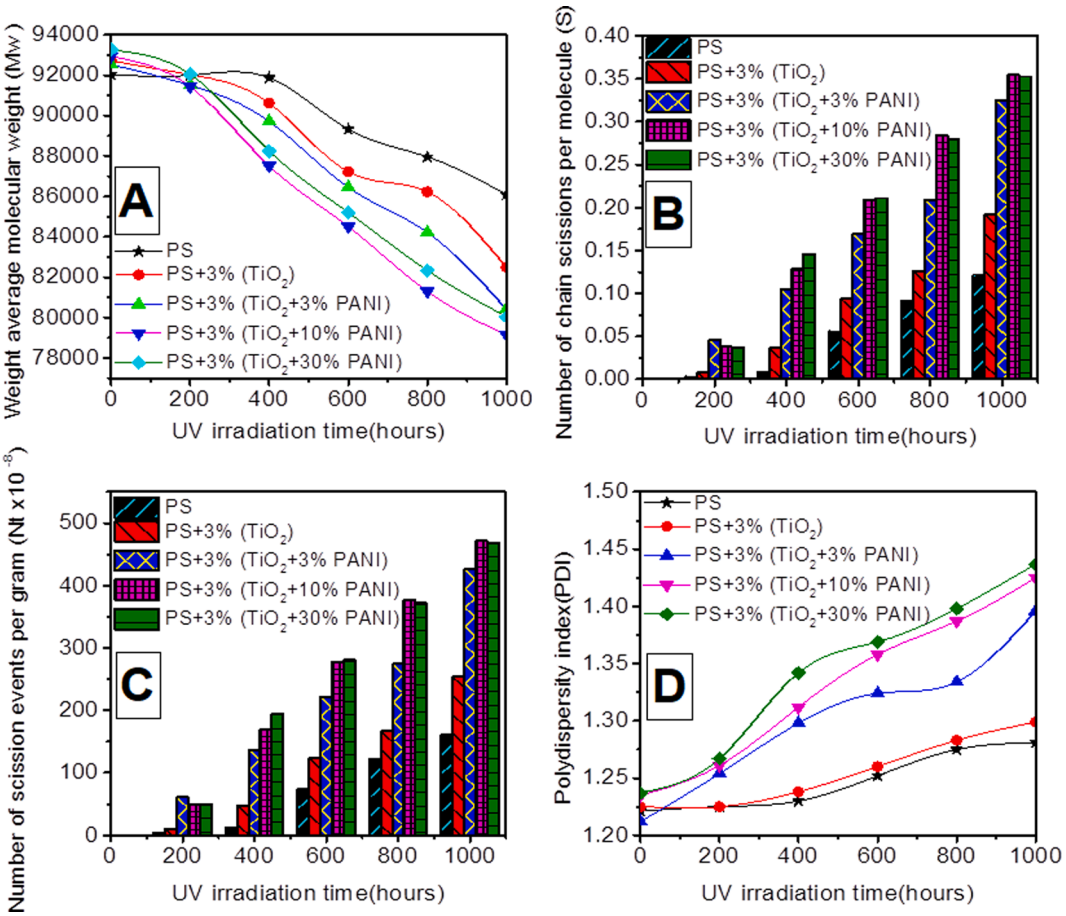

Fig. 5. A) Weight average molecular weight ($\overline{M}_w$), **B)** Number of chain scissions per molecule (S), **C)** number of scission events per gram(N_t) and **D**) Polydispersity index (PDI) of PS and PS-composite under different UV irradiation time.

$$S = \left[\left(\overline{M}_n\right)_0/\left(\overline{M}_n\right)_t\right] - 1 \quad (3)$$

$$N_t = \left[\frac{1}{(M_n)_t}\right] - \left[\frac{1}{(M_n)_0}\right] \quad (4)$$

$$PDI = \frac{\overline{M}_w}{\overline{M}_n} \quad (5)$$

Where $\left(\overline{M}_n\right)_0$ represents number average molecular weight before UV irradiation and $\left(\overline{M}_n\right)_t$ represents the same after UV irradiation of 't' hours.

S and N_t of PS and PS-composites increased with respect to UV irradiation time (Fig. 5 B and C). This is a clear indication of increasing chain scission on UV exposure. PS-TiO_2-PANI composites underwent better chain scission compared to PS and PS-TiO_2. It is therefore understood that TiO_2-PANI composites enhanced the chain scission of PS matrix compared to TiO_2 under UV radiation. Chain scission was predominant in PS-3% (TiO_2-10% PANI) compared to other PS-TiO_2-PANI composites. The PDI of the specimens also increased upon UV irradiation (Fig. 5 D). The maximum increase in PDI was observed for PS-TiO_2-PANI composites. The increase in the value of PDI suggests that the chain scission occurred in a random fashion upon UV irradiation. PS-TiO_2-PANI composites underwent better decrease in the average molecular weights as well as better chain scission with respect to UV irradiation compared to PS-TiO_2 and PS. The extent of chain scission observed in PS-TiO_2-PANI composites followed the order PS+(TiO_2 + 10% PANI) > PS+(TiO_2 + 30% PANI) > PS+(TiO_2 + 3% PANI). It could be concluded that the optimum percentage of PANI in PS-TiO_2-PANI composites for effective chain scission under UV radiation is ≈10%.

ATR-FTIR spectroscopy was used to investigate the chemical changes taking place in the PS and PS-composites after UV irradiation. PS, PS-TiO_2 and PS-TiO_2-PANI composites were monitored using ATR-FTIR spectroscopy at regular intervals of UV irradiation. The IR spectra of all the PS composite exhibited new bands on UV irradiation of 200 h, between the ranges 1740–1680 cm^{-1} and 1680–1650 cm^{-1} that could be attributed to carbonyl (>C = O) and alkenic double bonds (>C = C <) stretching frequencies respectively. > C = O stretching vibration arise from the carbonyl compounds (aldehydes or ketones) formed as a result of carbon–oxygen bonds formed between the polymer chain and adsorbed oxygen (as discussed in section 4, mechanism). The observed > C = C < stretching vibrations reveals the formation of alkenes as a result of UV initiated homolytic cleavage of C-H bonds wihin the PS chain. A remarkable increase in the absorption intensities of these bands were observed upon further UV exposure. An increase in the intensities of IR absorption bands were also observed between the frequency ranges 4000–3500 cm^{-1} and 1630–1600 cm^{-1} that could be attributed to hydroxyl/ hydroperoxy (–OH /–OOH) and conjugated carbon double bond stretching frequency respectively. Formation of alcohols and hydroperoxides as a result of interaction of PS chain with superoxide or hydroxyl radicals could be concluded. The formation of conjugated bond occurs as a result of C-H bond cleavage as discussed in section 4. These observations confirm that the PS composites underwent photo-oxidation in the presence of UV radiation. FTIR spectra further revealed that the characteristic bands of phenyl ring (centred at 691 cm^{-1}, 752 cm^{-1}, 905 cm^{-1} and 1027 cm^{-1} due to the C-H out of plane bend and at 1448 cm^{-1} due to aromatic carbon–carbon double bond stretch) endured no

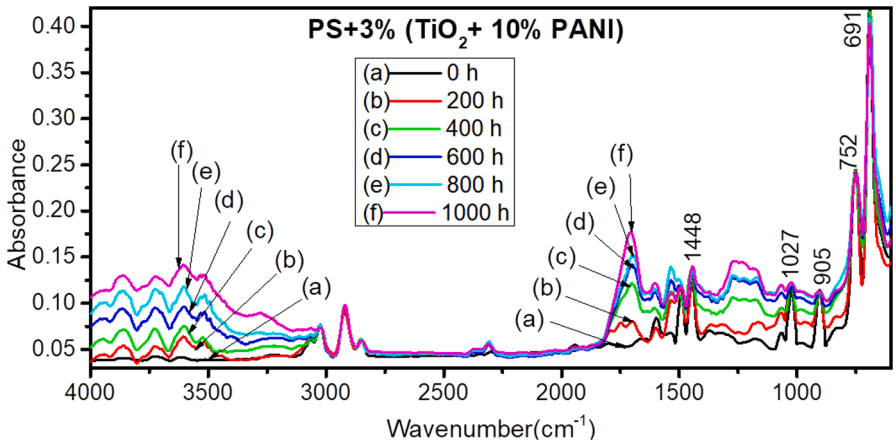

Fig. 6. FTIR spectra of PS+(TiO_2 + 10% PANI) composite after different UV exposure time intervals ranging from 0 h to 1000 h.

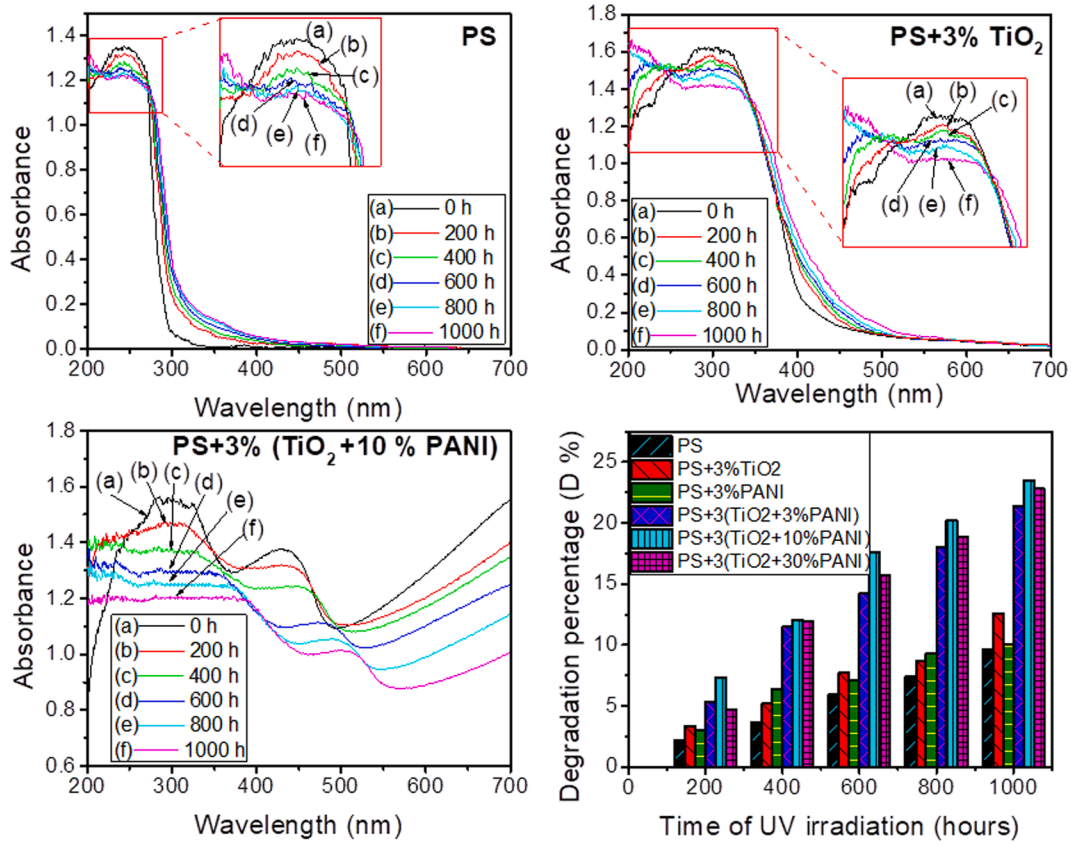

Fig. 7. UV-DRS of PS, PS + 3% TiO_2, PS-(TiO_2-10% PANI) composites and their degradation percentages at different UV exposure time intervals ranging from 0 h to 1000 h.

observable changes on UV exposure. This observation discloses the fact that the phenyl ring of PS remained intact and the photo-oxidation have affected only the polymer chain of the PS matrix. An overview of IR spectra of PS and all the PS-composites revealed that the extent of photo-oxidative degradation was greater in PS-TiO_2-PANI composites compared to pristine PS (Fig. S4) and PS-TiO_2 composite (Fig. S5). PS-(TiO_2-10% PANI) underwent better photo-oxidation among the PS-TiO_2-PANI composites under study (Fig. 6). (Refer Fig. S6 and S7 for the FTIR spectra of PS-(TiO_2-3% PANI) and PS-(TiO_2-30% PANI) respectively).

The UV-DRS absorption spectra of pristine PS showed absorption only in the UV region (between 200 and 300 nm), caused by the combined absorption of phenyl rings in PS matrix. PS-TiO_2 also absorbed only in the UV region due to the absorbance of UV light by the electrons in the valence bands of TiO_2, in addition to the characteristic absorption of PS. UV–visible spectra of PS-PANI as well as PS-TiO_2-PANI composites (Fig. 7) showed absorption bands with two absorption maxima between the wavelengths 230–350 nm (UV region), 400–500 nm (visible region) and a "tail band" starting from around 500 nm and extending to far-red region. As the time of UV irradiation increases, decrease in absorption intensities were noticed for all the PS composites under study. The decrease in absorption bands observed in the UV region of PS and PS-composites arise due to the photodegradation of PS matrix on UV exposure. As the time of UV radiation increased from 0 to 1000 h, absorption maxima in the UV region decreased appreciably. The decrease

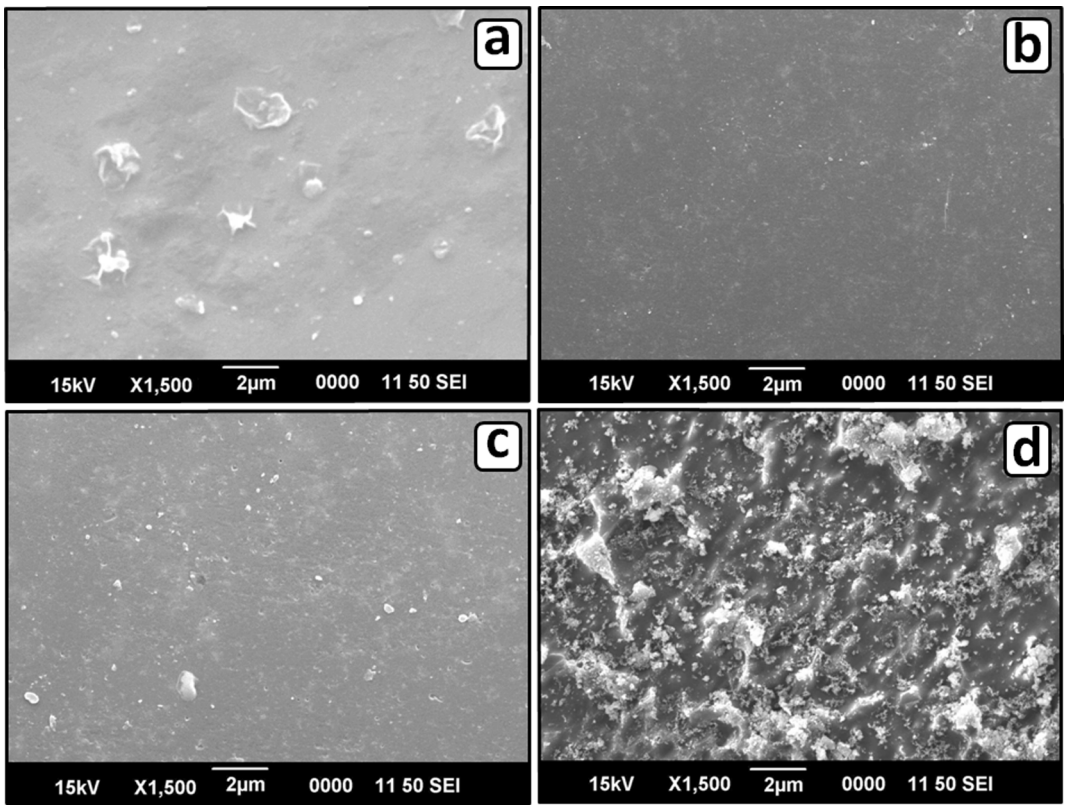

Fig. 8. SEM image of PS + 3% PANI (a), PS + 3%TiO_2 (b) and PS + 3%(TiO_2 + 10% PANI)(c) before UV irradiation and PS + 3%(TiO_2 + 10% PANI)(d) after UV irradiation of 1000 h.

in UV absorption was greater for PS-TiO_2 composites compared to pristine PS. PS-TiO_2-PANI composites showed still greater decrease in UV absorption compared to PS-TiO_2 composites, that highlights better photocatalytic activity of TiO_2-PANI compared to pristine PANI for the photodegradation of PS. Maximum decrease was however observed in PS + 3% (TiO_2 + 10%PANI) (Fig. 7) compared to PS + 3%PANI, PS + 3% (TiO_2 + 3%PANI) and PS + 3% (TiO_2 + 30%PANI) (Fig. S8). Slight red shift in the absorption bands was also noticed. The red shift may be due to the absorption of partially degraded PS in the visible region. Formation of conjugated double bonds as observed in the FTIR spectra (discussed in section 4, mechanism) may be considered. Degradation percentage (D%) of the composites were determined from UV-DRS using equ 6.

$$D\% = \left[\frac{(A_0 - A_t)}{A_0}\right] \times 100 \quad (6)$$

Where, A_0 and A_t denotes the absorbance before and after time t of UV irradiation respectively.

D% of PS-TiO_2-PANI composites were found to be higher compared to PS-TiO_2 and PS. D% was maximum in PS-(TiO_2-10% PANI) (Fig. 7) among the PS-TiO_2-PANI composites.

SEM image of PS + 3% PANI composite showed some aggregations of PANI over PS matrix (Fig. 8a). Dispersion of TiO_2 in PS matrix was uniform without many aggregations in PS + 3% TiO_2 composite (Fig. 8b). Dispersion of TiO_2 + 30% PANI within PS matrix was found to be more uniform compared to that of PANI over the PS matrix (Fig. 8c). All the PS-composites showed increased surface roughness after 1000 h of UV irradiation due to surface degradation. Fig. 8d shows PS + 3% (TiO_2 + 10% PANI) composite with increased surface roughness after 1000 h of UV exposure.

Thermogravimetric analysis (TGA) conducted in nitrogen atmosphere for all the PS composites showed two stages of weight loss curves attributing to the desorption of water molecules and decomposition of the composites (Fig. 9). Decomposition temperature of PS observed at around 252 °C increased to 272 °C for PS + 3% TiO_2 composite and further to 290 °C for PS + 3%(TiO_2 + 10% PANI). Enhanced thermal stability PS, on TiO_2 and TiO_2 + PANI loading is evident here. Decomposition temperatures of UV irradiated PS and PS-composites decreased appreciably after UV irradiation. This implies that UV irradiation has affected the polymer chain adversely leading to its depletion. Reduced thermal stability of the composites due to photodegradation in the presence of UV radiation could be concluded.

Flexural and tensile properties of PS were improved on TiO_2 and TiO_2-PANI loading. Fig. 10 A1& A2 represents flexural and tensile strengths of pristine PS, PS + 3%TiO_2 PS + 3% PANI and PS-TiO_2-PANI composites. Mechanical strength of PS-PANI composite was lower than that of PS-TiO_2 probably due to the aggregations of PANI which prevented uniform dispersion along the PS matrix (as evident from SEM image- Fig. 8 above), forming defective voids. PS-TiO_2-PANI composites exhibited superior mechanical properties compared to PS-TiO_2. Maximum tensile and flexural strengths were observed in PS-(TiO_2-10% PANI) composite. Higher percentage of PANI in the composites, however, decreased their mechanical strength. Flexural (Fig. 10 B1) and tensile (Fig. 10 B2) strength of all the PS composites decreased on UV irradiation. Deterioration of the polymer chain caused by photodegradation, decreased the mechanical strength of polymer composites, under UV radiation. It was also clear from Fig. 10 B1 & B2 that PS+ (TiO_2 + 10% PANI) composite underwent maximum decrease in tensile and flexural strengths upon UV irradiation.

Breakdown voltage (BDV) of PS-TiO_2-PANI composites (Fig. 11 A) measured in alternating current frequency 50 Hz, were found to be lower compared to that of PS and PS-TiO_2 composite. Decrease in the value of BDV observed in these composites could be due to the conducting nature of PANI. The value of BDV decreased as the percentage of PANI in the composites increased. BDV measured for PS and PS-3%TiO_2 composites were 25.17 KV/mm and 30.03 KV/mm respectively. The

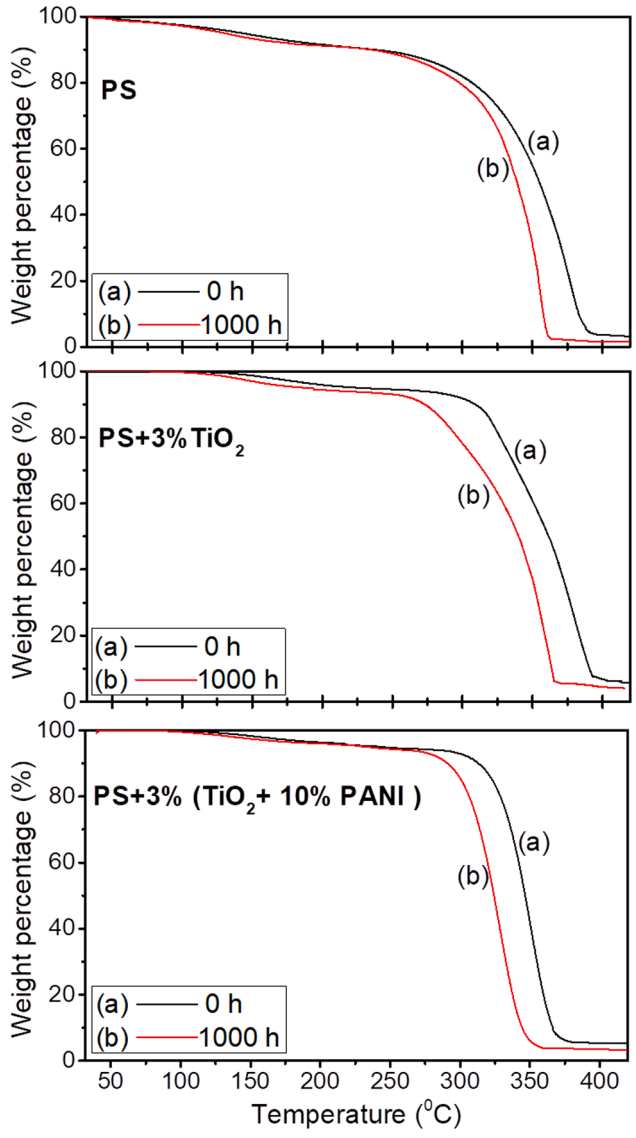

Fig. 9. Thermogram of PS, PS + 3%TiO_2 and PS + 3%(TiO_2 + 10% PANI) before(a) and after (b) UV irradiation of 1000 h obtained through TGA.

values of BDV of PS-TiO_2-PANI composites were 21.3 KV/mm for PS + 3%(TiO_2 + 3% PANI, 18.78 KV/mm for PS + 3%(TiO_2 + 10% PANI) and 14.85 KV/mm for PS + 3%(TiO_2 + 30% PANI).

BDV values of all these composites further decreased as the time of UV irradiation increased. The decrease in BDV upon UV irradiation could be due to the formation of charge centres during photodegradation of the composites. PS + 3%(TiO_2 + 10% PANI) underwent better decrease in BDV values upon UV irradiation compared to the other composites under study.

Capacitance of PS, PS-TiO_2 and PS-TiO_2-PANI composites was measured (within the frequency range 0 to 10^7 Hz). Dielectric permittivity (ε_r) of the composites was calculated from capacitance using the following expression (equ. 7).

$$C = \varepsilon_r \varepsilon_0 \left(\frac{A}{t}\right) \quad (7)$$

Where, 'C' is the Capacitance; 'ε_r' is the dielectric permittivity of polymer specimens; 'ε_0' is the dielectric permittivity of free space (ε_0= 8.854 × 10^{-12}F/m); 'A' and 't' represents the area and thickness of the polymer specimens.

ε_r of the composites increased as the percentage of PANI in the composites increased (Fig. 11 B). ε_r of the composites further increased upon UV irradiation. This could be due to the formation of polarisable species in PS matrix as a consequence of photodegradation (Fig. 11 C).

All the PS-composite specimens underwent a considerable weight loss as the time of UV irradiation increased. The observed weight loss could be due to the formation and evolution of volatile gases like CO, CO_2, H_2O, H_2 etc during photodegradation. PS-TiO_2-PANI composites underwent better weight loss on UV irradiation. The order of weight loss observed is as follows PS + 3%(TiO_2 + 10% PANI) > PS + 3%(TiO_2 + 30% PANI) > PS + 3%(TiO_2 + 3% PANI) > PS + 3% TiO_2 > PS + 3% PANI > PS. The order of weight loss observed was in accordance with the order of photodegradation observed in the previous results.

4. Mechanism of photodegration of PS and PS-composites

PS undergoes UV initiated photodegradation by transferring the triplet energy from their phenyl rings into the associated polymer chain backbones. Absorption of UV radiation causes an excitation of the phenyl rings of PS into singlet excited state (^{1}Ph*) and then into triplet excited state (^{3}Ph*) after inter system crossing (ISC). The triplet energy of phenyl ring is transferred into the polymer chain resulting in homolytic bond fission (-C-C-, C-H and/or Ph-C bond cleavage) and formation of macromolecular radical. Decrease in $\overline{M}_w$ and$\overline{M}_n$ as well as increase in the chain scissions were evident from GPC analysis. The extent of degradation of PS entirely depends upon the propagation of the radicals from the UV exposed polymer surface into the inner matrix. The notable changes in mechanical strength, thermal stability and electrical properties of the polymer specimens prove that the degradation has taken place throughout the matrix (and not limited to the polymer surface).

The formation and increase in the intensities of IR stretching vibrations corresponding to the –OH/–OOH, >C = O, >C = C < and conjugated carbon double bonds upon UV irradiation of PS specimens, confirm photo-oxidation. The characteristic IR absorption bands of phenyl rings were however not influenced by the UV radiation. We could conclude that the photo-oxidation has occurred only on the polymer chain backbone while the phenyl rings remained intact. The PS macromolecular radicals interact with the adsorbed atmospheric oxygen resulting in the formation of –OH, –OOH, >C = O groups covalently bonded to the polymer carbon chain. The formation of > C = C < and conjugated carbon double bonds in the polymer chain can also take place. The elimination of hydrogen radicals ($H^\bullet$) from the adjacent carbon results in the formation of π-bond between them. More such π-bonds formed between the carbon atoms may also result in conjugated double bonds. The formation of conjugated double bonds gave a slight yellow colouration to the composites. The red shift in the UV absorprion bands of the composites too supports conjugate double bond formation.

Nano TiO_2 loaded PS underwent better photodegradation compared to pristine PS under UV irradiation. UV radiation with energy exceeding the band gap energy of TiO_2 causes excitation the electrons from its valence band (VB) to the conduction band (CB). The electrons in the CB interact with the oxygen molecules generating superoxide radicals ($O_2^{\bullet-}$). The holes left behind in the VB interact with the adsorbed water molecules generating hydroxyl radicals ($OH^\bullet$). These reactive species further interacts with PS inorder to accelerate the rate of photodegradation.

The photocatalytic activity of nano TiO_2 was appreciably enhanced when coupled with PANI. The enhancement in photocatalytic activity could be explained on the basis of high efficiency of charge separation accomplished by synergetic effect of TiO_2 with PANI. The energies of the highest occupied molecular orbital (HOMO) of PANI lie between the VB and CB of TiO_2. The holes left behind in the VB of TiO_2 are transferred to the HOMO of PANI. Chance for recombination of the electrons with the holes is hence minimized[19,47–49]. The minimised recombination of photogenerated charges within TiO_2 furnished by its association with PANI increased its photocatalytic efficiency for the degradation of PS

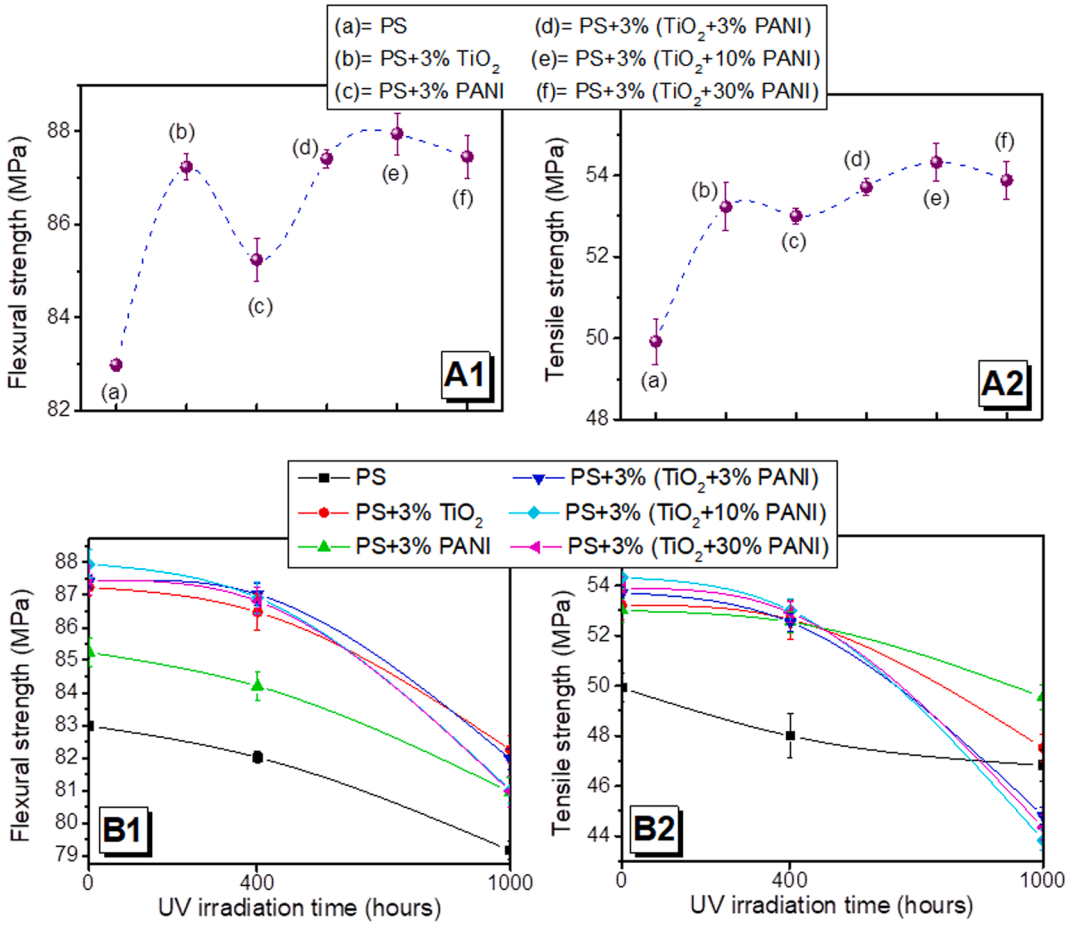

Fig. 10. Flexural and tensile strength of PS and PS-composites before UV irradiation (A1& A2) and at UV irradiation intervals of 400 and 1000 h (B1& B2).

under UV radiation.

5. Conclusion

TiO_2-PANI composites were successfully developed using chemical oxidative polymerization. The crystal phase of nano TiO_2 remained intact even after coupling with PANI. FTIR spectra of the composites revealed the existence of strong molecular interactions between PANI and nano TiO_2. UV-DRS showed that the TiO_2-PANI composites could absorb UV and visible region of spectra. Increased percentage of PANI coupling, decreased the optical band gap energy within the composites. The composites exhibited crystalline morphology and existed in nano dimensions, without much aggregation. Photodegradation of PS was appreciably accelerated upon TiO_2-PANI loading, compared to PS-TiO_2 composite as well as pristine PS, under UV radiation. Better decrease in the average molecular masses reflecting faster chain scission, along with enhanced photo-oxidation, observed in PS-TiO_2-PANI composites proved the ability of TiO_2-PANI composites to act as better photocatalysts compared to pristine TiO_2 under UV radiation. Mechanical strength of PS improved considerably when loaded with TiO_2 and TiO_2-PANI. Among the PS-TiO_2-PANI composites, maximum tensile and flexural strengths was observed in PS + 3%(TiO_2 + 10% PANI). Further increase in the percentage of PANI, decreased the mechanical strengths of the composites. PS-TiO_2-PANI composites also showed accelerated mechanical deterioration upon UV irradiation. Formation of charged centres or polarisable groups, within the PS composite matrix, was evident from the decrease in BDV as well as increase in dielectric permittivity of the UV exposed composites. TGA results established that the thermal stability of the PS-composites decreases, when exposed to UV radiation. Weight loss as well as increase in surface roughness was observed in the PS-composites as an outcome of photodegradation. PS + 3%(TiO_2 + 10% PANI) underwent maximum photodegradation under UV radiation compared to the other PS-composites. Photocatalytic activity of PS-composite with 30% PANI was not as efficient as that with 10% PANI. This trend could be due aggregation of excess PANI in composite with 30% PANI, that has an adverse impact in its photochemistry. Surface modification of nano TiO_2 with PANI, improved its photocatalytic efficiency for the photodegradation of PS appreciably under UV radiation. The present investigation holds further scope for the study of photodegradation of PS using TiO_2-PANI photocatalysts under visible radiation

CRediT authorship contribution statement

S. Dinoop lal: Conceptualization, Formal analysis, Investigation, Data curation, Writing - original draft, Methodology, Software, Visualization. **T. Sunil Jose:** Conceptualization, Project administration, Supervision, Writing - review & editing, Data curation, Methodology, Visualization. **C. Rajesh:** Resources, Conceptualization, Methodology, Validation. **P. Anju Rose Puthukkara:** Formal analysis, Investigation, Methodology, Software. **K. Savitha Unnikrishnan:** Formal analysis, Investigation, Methodology, Software. **K.J. Arun:** Resources, Methodology, Software, Validation.

Declaration of Competing Interest

The authors declare that they have no known competing financial interests or personal relationships that could have appeared to influence the work reported in this paper.

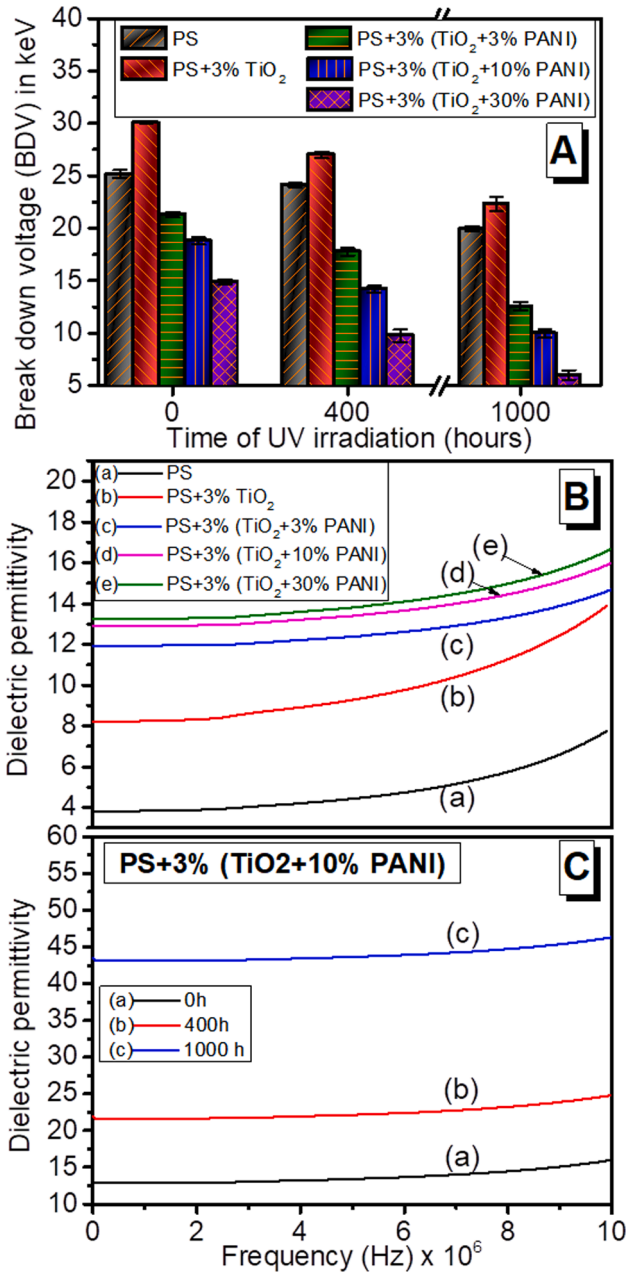

Fig. 11. Breakdown voltage (BDV) of PS-composites at varying UV irradiation time intervals (A). Dielectric permittivity versus frequency of PS-composites before UV irradiation (B) and Dielectric permittivity versus frequency of PS + 3%(TiO_2 + 10%PANI) composites at varying UV irradiation time intervals (C).

Acknowledgement

The authors wish to acknowledge SAIF-STIC, Cochin University of Science and Technology (CUSAT), India, National Institute of Science and Technology, Calicut, India and CSIR-Central Electrochemical Research Institute, Karaikudi, India for their valuable support.

Data availability

The raw/processed data required to reproduce these findings cannot be shared at this time as the data also forms part of an ongoing study.

Appendix A. Supplementary data

Supplementary data to this article can be found online at https://doi.org/10.1016/j.eurpolymj.2021.110493.

References

[1] K.F. Mulder, Sustainable Consumption and Production of Plastics? Technol. Forecast. Soc. Change. 58 (1998) 105–124, https://doi.org/10.1016/S0040-1625(97)00129-7.
[2] R. Geyer, J.R. Jambeck, K.L. Law, Production, use, and fate of all plastics ever made, Sci. Adv. 3 (2017), https://doi.org/10.1126/sciadv.1700782.
[3] S.K. Tulashie, E.K. Boadu, F. Kotoka, D. Mensah, Plastic wastes to pavement blocks: A significant alternative way to reducing plastic wastes generation and accumulation in Ghana, Constr. Build. Mater. 241 (2020) 118044. https://doi.org/https://doi.org/10.1016/j.conbuildmat.2020.118044.
[4] W.C. LI, H.F. Tse, L. Fok, Plastic waste in the marine environment: A review of sources, occurrence and effects, Sci. Total Environ. 566–567 (2016) 333–349. https://doi.org/https://doi.org/10.1016/j.scitotenv.2016.05.084.
[5] B.G. Kwon, K. Saido, K. Koizumi, H. Sato, N. Ogawa, S.-Y. Chung, T. Kusui, Y. Kodera, K. Kogure, Regional distribution of styrene analogues generated from polystyrene degradation along the coastlines of the North-East Pacific Ocean and Hawaii, Environ. Pollut. 188 (2014) 45–49. https://doi.org/https://doi.org/10.1016/j.envpol.2014.01.019.
[6] B. Gewert, M. Plassmann, O. Sandblom, M. MacLeod, Identification of Chain Scission Products Released to Water by Plastic Exposed to Ultraviolet Light, Environ. Sci. Technol. Lett. 5 (2018) 272–276, https://doi.org/10.1021/acs.estlett.8b00119.
[7] E. Yousif, R. Haddad, Photodegradation and photostabilization of polymers, especially polystyrene: review, Springerplus. 2 (2013) 1–32, https://doi.org/10.1186/2193-1801-2-398.
[8] J. Madhavan, P.S. Sathish Kumar, S. Anandan, F. Grieser, M. Ashokkumar, Sonophotocatalytic degradation of monocrotophos using TiO2 and Fe3+, J. Hazard. Mater. 177 (2010) 944–949, https://doi.org/10.1016/j.jhazmat.2010.01.009.
[9] M.M. Khan, S.F. Adil, A. Al-Mayouf, Metal oxides as photocatalysts, J. Saudi Chem. Soc. 19 (2015) 462–464. https://doi.org/https://doi.org/10.1016/j.jscs.2015.04.003.
[10] D. lal S, S.J. T, R. C, Solid-phase photodegradation of polystyrene by nano TiO2 under ultraviolet radiation, Environ. Nanotechnology, Monit. Manag. 12 (2019) 100229. https://doi.org/https://doi.org/10.1016/j.enmm.2019.100229.
[11] D. Hwang, Y. Shul, Y. Chu, Photodegradation behavior of the polycarbonate/TiO2 composite films under the UV irradiation in ambient air condition, Polym. Compos. 36 (2014) 1462–1468, https://doi.org/10.1002/pc.23052.
[12] R.T. Thomas, V. Nair, N. Sandhyarani, TiO2 nanoparticle assisted solid phase photocatalytic degradation of polythene film: A mechanistic investigation, Colloids Surfaces A Physicochem. Eng. Asp. 422 (2013) 1–9, https://doi.org/10.1016/j.colsurfa.2013.01.017.
[13] A. Fujishima, X. Zhang, D.A. Tryk, TiO2 photocatalysis and related surface phenomena, Surf. Sci. Rep. 63 (2008) 515–582. https://doi.org/https://doi.org/10.1016/j.surfrep.2008.10.001.
[14] U. Riaz, S.M. Ashraf, J. Kashyap, Enhancement of photocatalytic properties of transitional metal oxides using conducting polymers: A mini review, Mater. Res. Bull. 71 (2015) 75–90, https://doi.org/10.1016/j.materresbull.2015.06.035.
[15] F. Chen, W. An, Y. Li, Y. Liang, W. Cui, Fabricating 3D porous PANI/TiO2–graphene hydrogel for the enhanced UV-light photocatalytic degradation of BPA, Appl. Surf. Sci. 427 (2018) 123–132. https://doi.org/https://doi.org/10.1016/j.apsusc.2017.08.146.
[16] M.O. Ansari, M.M. Khan, S.A. Ansari, M.H. Cho, Polythiophene nanocomposites for photodegradation applications: Past, present and future, J. Saudi Chem. Soc. 19 (2015) 494–504. https://doi.org/https://doi.org/10.1016/j.jscs.2015.06.004.
[17] M.O. Ansari, M.M. Khan, S.A. Ansari, K. Raju, J. Lee, M.H. Cho, Enhanced Thermal Stability under DC Electrical Conductivity Retention and Visible Light Activity of Ag/TiO2@Polyaniline Nanocomposite Film, ACS Appl. Mater. Interfaces. 6 (2014) 8124–8133, https://doi.org/10.1021/am500488e.
[18] A. lui Olad, S. Behboudi, A. li A. Entezami, Preparation, characterization and photocatalytic activity of TiO2/polyaniline core-shell nanocomposite, Bull. Mater. Sci. 35 (2012) 801–809. https://doi.org/10.1007/s12034-012-0358-7.
[19] E. Asgari, A. Esrafili, A.J. Jafari, R.R. Kalantary, H. Nourmoradi, M. Farzadkia, The comparison of ZnO/polyaniline nanocomposite under UV and visible radiations for decomposition of metronidazole: Degradation rate, mechanism and mineralization, Process Saf. Environ. Prot. 128 (2019) 65–76, https://doi.org/10.1016/j.psep.2019.05.050.
[20] Y. Ma, M. Ma, X. Yin, Q. Shao, N. Lu, Y. Feng, Y. Lu, E.K. Wujcik, X. Mai, C. Wang, Z. Guo, Tuning polyaniline nanostructures via end group substitutions and their morphology dependent electrochemical performances, Polymer (Guildf). 156 (2018) 128–135, https://doi.org/10.1016/j.polymer.2018.09.051.
[21] S.N. Botewad, V.G. Pahurkar, G.G. Muley, Fabrication and evaluation of evanescent wave absorption based polyaniline-cladding modified fiber optic urea biosensor, Opt. Fiber Technol. 40 (2018) 8–12, https://doi.org/10.1016/j.yofte.2017.11.002.
[22] L. He, B. Cui, J. Liu, Y. Song, M. Wang, D. Peng, Z. Zhang, Novel electrochemical biosensor based on core-shell nanostructured composite of hollow carbon spheres and polyaniline for sensitively detecting malathion, Sensors Actuators B Chem. 258 (2018) 813–821, https://doi.org/10.1016/j.snb.2017.11.161.
[23] V.C. Anitha, A.N. Banerjee, S.W. Joo, Recent developments in TiO2 as n- and p-type transparent semiconductors: synthesis, modification, properties, and energy-

related applications, J. Mater. Sci. 50 (2015) 7495–7536, https://doi.org/10.1007/s10853-015-9303-7.
[24] F. Yakuphanoglu, B.F. Şenkal, Electronic and Thermoelectric Properties of Polyaniline Organic Semiconductor and Electrical Characterization of Al/PANI MIS Diode, J. Phys. Chem. C. 111 (2007) 1840–1846, https://doi.org/10.1021/jp0653050.
[25] R. Ganesan, A. Gedanken, Organic-organic hybrid materials based on polyaniline/TiO2 nanocomposites for ascorbic acid fuel cell systems, Nanotechnology. 19 (2008), 435709, https://doi.org/10.1088/0957-4484/19/43/435709.
[26] V. Gilja, K. Novaković, J. Travas-Sejdic, Z. Hrnjak-Murgić, M.K. Roković, M. Žic, Stability and synergistic effect of polyaniline/TiO2 photocatalysts in degradation of azo dye in wastewater, Nanomaterials. 7 (2017) 412, https://doi.org/10.3390/nano7120412.
[27] V. Gilja, I. Vrban, V. Mandić, M. Žic, Z. Hrnjak-Murgić, Preparation of a PANI/ZnO composite for efficient photocatalytic degradation of acid blue, Polymers (Basel). 10 (2018) 940. https://doi.org/https://doi.org/10.3390/polym10090940.
[28] R. Saravanan, E. Sacari, F. Gracia, M.M. Khan, E. Mosquera, V.K. Gupta, Conducting PANI stimulated ZnO system for visible light photocatalytic degradation of coloured dyes, J. Mol. Liq. 221 (2016) 1029–1033. https://doi.org/https://doi.org/10.1016/j.molliq.2016.06.074.
[29] S. Min, F. Wang, Y. Han, An investigation on synthesis and photocatalytic activity of polyaniline sensitized nanocrystalline TiO2 composites, J. Mater. Sci. 42 (2007) 9966–9972, https://doi.org/10.1007/s10853-007-2074-z.
[30] G.K.R. Senadeera, T. Kitamura, Y. Wada, S. Yanagida, Deposition of polyaniline via molecular self-assembly on TiO2 and its uses as a sensitiser in solid-state solar cells, J. Photochem. Photobiol. A Chem. 164 (2004) 61–66. https://doi.org/https://doi.org/10.1016/j.jphotochem.2003.12.026.
[31] S.-J. Tang, A.-T. Wang, S.-Y. Lin, K.-Y. Huang, C.-C. Yang, J.-M. Yeh, K.-C. Chiu, Polymerization of aniline under various concentrations of APS and HCl, Polym. J. 43 (2011) 667–675, https://doi.org/10.1038/pj.2011.43.
[32] N.Y. Abu-Thabit, Chemical Oxidative Polymerization of Polyaniline: A Practical Approach for Preparation of Smart Conductive Textiles, J. Chem. Educ. 93 (2016) 1606–1611, https://doi.org/10.1021/acs.jchemed.6b00060.
[33] Y. Bu, Z. Chen, Role of Polyaniline on the Photocatalytic Degradation and Stability Performance of the Polyaniline/Silver/Silver Phosphate Composite under Visible Light, ACS Appl. Mater. Interfaces. 6 (2014) 17589–17598, https://doi.org/10.1021/am503578s.
[34] A. Olad, N. Asadi, S. Mohammadi, A. Rahimeh, The use of adsorption method to preparation of polyaniline / ZnO nanocomposite varistor, J. Mater. Sci. Mater. Electron. 29 (2018) 9692–9699, https://doi.org/10.1007/s10854-018-9006-3.
[35] K. Raghava, K.V. Karthik, S.B.B. Prasad, S.K. Soni, H.M. Jeong, Enhanced photocatalytic activity of nanostructured titanium dioxide / polyaniline hybrid photocatalysts Enhanced photocatalytic activity of nanostructured titanium dioxide / polyaniline hybrid photocatalysts, Polyhedron. 120 (2016) 169–174, https://doi.org/10.1016/j.poly.2016.08.029.
[36] D. lal S, S.J. T, R. C, A. KJ, Accelerated Photodegradation of Solid Phase Polystyrene by Nano TiO2-Graphene Oxide Composite under Ultraviolet radiation, Polym. Degrad. Stab. 184 (2021) 109476. https://doi.org/https://doi.org/10.1016/j.polymdegradstab.2020.109476.
[37] V. Talwar, O. Singh, R.C. Singh, ZnO assisted polyaniline nanofibers and its application as ammonia gas sensor, Sensors Actuators B Chem. 191 (2014) 276–282, https://doi.org/10.1016/j.snb.2013.09.106.
[38] J.P. Pouget, C.-H. Hsu, A.G. Mac Diarmid, A.J. Epstein, Structural investigation of metallic PAN-CSA and some of its derivatives, Synth. Met. 69 (1995) 119–120. https://doi.org/https://doi.org/10.1016/0379-6779(94)02382-9.
[39] M.L. Singla, S. Awasthi, A. Srivastava, D.V.S. Jain, Effect of doping of organic and inorganic acids on polyaniline/Mn3O4 composite for NTC and conductivity behaviour, Sensors Actuators A Phys. 136 (2007) 604–612. https://doi.org/https://doi.org/10.1016/j.sna.2006.12.002.
[40] B.S. Singu, P. Srinivasan, S. Pabba, Benzoyl Peroxide Oxidation Route to Nano Form Polyaniline Salt Containing Dual Dopants for Pseudocapacitor, J. Electrochem. Soc. 159 (2011) A6–A13, https://doi.org/10.1149/2.036201jes.
[41] W. Feng, E. Sun, A. Fujii, H. Wu, K. Niihara, K. Yoshino, Synthesis and Characterization of Photoconducting Polyaniline-TiO2 Nanocomposite, Bull. Chem. Soc. Jpn. 73 (2000) 2627–2633, https://doi.org/10.1246/bcsj.73.2627.
[42] H. Xia, Q. Wang, Ultrasonic Irradiation: A Novel Approach To Prepare Conductive Polyaniline/Nanocrystalline Titanium Oxide Composites, Chem. Mater. 14 (2002) 2158–2165, https://doi.org/10.1021/cm0109591.
[43] H. Arami, M. Mazloumi, R. Khalifehzadeh, S.K. Sadrnezhaad, Sonochemical preparation of TiO2 nanoparticles, Mater. Lett. 61 (2007) 4559–4561. https://doi.org/https://doi.org/10.1016/j.matlet.2007.02.051.
[44] A.A. Khan, M. Khalid, Synthesis of Nano-Sized ZnO and Polyaniline-Zinc Oxide Composite : Characterization, Stability in Terms of DC Electrical Conductivity Retention and Application in Ammonia Vapor Detection, Appl. Polym. 117 (2010) 1601–1607, https://doi.org/10.1002/app.32037.
[45] M. Sawarkar, S.A. Pande, P.S. Agrawal, Synthesis and characterization of polyaniline doped metal oxide nanocomposites, Int. Res. J. Eng. Technol. 9 (2015) 2427–2432.
[46] X. Zhang, Q. Wang, L.-H. Zou, J.-W. You, Facile fabrication of titanium dioxide/fullerene nanocomposite and its enhanced visible photocatalytic activity, J. Colloid Interface Sci. 466 (2016) 56–61. https://doi.org/https://doi.org/10.1016/j.jcis.2015.12.013.
[47] A. Anand, N. Rani, P. Saxena, H. Bhandari, S.K. Dhawan, Development of polyaniline/zinc oxide nanocomposite impregnated fabric as an electrostatic charge dissipative material, Polym. Int. 64 (2015) 1096–1103, https://doi.org/10.1002/pi.4870.
[48] H. Zhang, R. Zong, J. Zhao, Y. Zhu, Dramatic Visible Photocatalytic Degradation Performances Due to Synergetic Effect of TiO2 with PANI, Environ. Sci. Technol. 42 (2008) 3803–3807, https://doi.org/10.1021/es703037x.
[49] H. Zhang, R. Zong, Y. Zhu, Photocorrosion Inhibition and Photoactivity Enhancement for Zinc Oxide via Hybridization with Monolayer Polyaniline, J. Phys. Chem. 113 (2009) 4605–4611, https://doi.org/10.1021/jp810748u.